Marine Pollution Bulletin 197 (2023) 115729

Contents lists available at ScienceDirect

Marine Pollution Bulletin

journal homepage: www.elsevier.com/locate/marpolbul

Marine oil spill photodegradation: Laboratory simulation, affecting factors analysis and kinetic model development

Pu Li, Zhenhua Lu, Shichun Zou, Lihua Yang *

Guangdong Provincial Key Laboratory of Marine Resources and Coastal Engineering, School of Marine Sciences, Sun Yat-sen University, Guangzhou 510275, China

ARTICLE INFO

Keywords:
Marine oil spill
Oil spill photodegradation
Oil weathering
Oil spill modelling

ABSTRACT

Photodegradation significantly influences marine oil spill behavior, yet its role remains underrepresented in current models, impairing predictive accuracy. Addressing this, our study rigorously examined oil properties and environmental determinants affecting marine oil spill photodegradation through laboratory simulations. We identified and quantified key factors and their interactions, noting particularly the positive influence of asphaltene and negative implications of oil density. We also discerned a negative correlation between n-alkane degradation and carbon numbers. Our findings underscored the pivotal roles of temperature and irradiance in photodegradation. All tested oils adhered to first-order kinetics, with rate constants ranging from 0.0348 to 0.0645 day^{-1}. Finally, we introduced a novel model incorporating temperature, irradiance and their interactions, ensuring reasonable simulations for marine oil spill photodegradation, fortifying marine oil spill management strategies.

1. Introduction

In recent decades, burgeoning population and economic expansion have catalyzed an upswing in marine petroleum exploration and development, concomitantly amplifying marine transportation and associated oil-related endeavors. Data spanning 1970–2022 reveal a global incidence of 1861 oil spills resulting from ship collisions, each liberating over 7 t of oil, with 470 instances classed as major spills, each discharging upwards of 700 t (ITOPF, 2023). Despite a notable downtrend in the probability of marine oil spills over the past decade, the ecological repercussions persist extensively; illustratively, trace residues of oil from the Deepwater Horizon catastrophe linger in specific environments a decade post-incident (Passow and Overton, 2021). This enduring impact underscores the imperative for meticulous scrutiny and management of factors influencing oil spill behavior and subsequent remediation in marine contexts.

Once oil is introduced into the marine environment, it undergoes a myriad of migration and transformation phases. These changes in the oil's composition and traits are termed as oil weathering processes. There are two primary categories: 1) physical processes which encompass evaporation, dissolution, and emulsification, and 2) biogeochemical processes like photodegradation and biodegradation (NRC, 2003). These processes determine the fate of the spilled oil and its potential environmental impact. While certain researchers have underscored the importance of photodegradation in the context of oil spills, particularly in their long-term weathering (Payne and Phillips, 1985), the bulk of oil spill scenarios have historically minimized its significance (Reed et al., 1999; NRC, 2003). This viewpoint was pivoted following the Deepwater Horizon oil spill. A confluence of field observations and laboratory simulations revealed that photodegradation swiftly emerged as the predominant weathering process in the post-spill period, illuminating a critical need to recalibrate understanding and approaches to evaluating oil spill impacts and mitigation strategies. Within a span ranging from hours to weeks after a spill, photodegradation transformed nearly half of the surface oil into oxygenated compounds (Hall et al., 2013; White et al., 2016; Ward et al., 2018). In detail, photodegradation results in partial oxidation of petroleum hydrocarbons. This produces a mix of ketones, aldehydes, acids, and various oxygenated derivatives. It can also trigger chemical reactions that cause bond breaks and polymerization, further affecting the oil transport and fate (Aeppli et al., 2018; Ward and Overton, 2020). Understanding these complex reactions is vital for predicting the long-term effects of spills and optimizing clean-up strategies. Moreover, photodegradation interplays with other weathering processes, such as dissolution, emulsification, and biodegradation (Zito et al., 2020; Aeppli et al., 2022).

The rate and extent of photodegradation in oil spills are influenced

* Corresponding author.
E-mail address: yanglih2@mail.sysu.edu.cn (L. Yang).

https://doi.org/10.1016/j.marpolbul.2023.115729
Received 22 August 2023; Received in revised form 23 October 2023; Accepted 26 October 2023
Available online 30 October 2023

by a combination of the oil's inherent physical and chemical properties and various environmental factors. Delving into the effects of oil properties, Yang et al. (2016) observed that crude oils with higher aromatic hydrocarbon contents degrade at significantly accelerated rates compared to their counterparts with lower aromatic content. Additionally, other studies have pinpointed sulfur and asphaltene contents as influential factors in the photodegradation process (Niles et al., 2020; Yang et al., 2022). Shifting focus to environmental determinants, a bulk of research has explored how these factors influence the photodegradation of polycyclic aromatic hydrocarbons (PAHs) in marine oil spills. Notably, Jing et al. (2014) examined the photodegradation of naphthalene in oily wastewater under variable temperatures. Their findings suggested that elevated temperatures enhanced the photodegradation of naphthalene. Meanwhile, other studies have probed into the roles of environmental cations and anions, such as Cu^{2+} and NO_3^-/NO_2^-. These ions can either act as radical quenchers or function as light-screening agents, thus modulating the photodegradation process of oil spills (Yang et al., 2008; Ji et al., 2012). The role of light, particularly its conditions and intensity, is paramount in oil spill photodegradation. In various simulation experiments, researchers have employed diverse light sources, from ultraviolet and mercury lamps to xenon lamps. The results from these experiments have underscored the significance of both ultraviolet and visible light in the degradation process (King et al., 2014; Arekhi et al., 2023). Despite these insights, the precise impacts of different factors, as well as their interdependencies, are yet to be fully grasped and quantified.

Understanding reaction kinetics is pivotal when examining marine oil spill photodegradation. Given the varied composition of oil spills, their photodegradation mechanisms can be intricate. Consequently, most current research targets a specific component of the oil spill to decipher its degradation pattern. For instance, Cai et al. (2017) reported that the photodegradation of anthracene and 9,10-dimethyl anthracene, especially in the presence of oil dispersants, adhered to first-order kinetics. This observation was mirrored by Bacosa et al. (2015), who found a similar kinetic pattern for n-alkanes, PAHs, and alkylated PAHs in oil spills. Yet, some research challenges this consensus. Notably, King et al. (2014) posited that the photodegradation of oil spills might not always follow first-order kinetics. Such conflicting findings underscore the complexity of degradation pathways and their dependency on multiple variables. Presently, the kinetics of oil spill photodegradation remains an unresolved question. This ambiguity has consequently led to a noticeable omission: the lack of photodegradation modules in contemporary oil spill models. While the majority of such models prioritize short-term predictions (typically <3 days) to guide emergency responses, there exists a pronounced need for a model adept at simulating chronic oil pollution over extended exposure durations, servicing other undertakings such as oil spill remediation and ecological risk assessments (Liubartseva et al., 2023). The neglect of photodegradation, underscored by Keramea et al. (2021), imperils the accuracy of marine oil spill projections, particularly in protracted temporal frames. Both field observations and laboratory tests have pointed towards the decreasing accuracy of oil spill models that do not incorporate photodegradation modules (Ward et al., 2018; Ward and Overton, 2020; Aeppli, 2022). Such discrepancies necessitate a more thorough exploration of photodegradation kinetics to refine predictive models.

To fill above gaps, this study aims to: 1) conduct a series of laboratory simulation experiments to investigate the influence of oil properties and environmental factors (e.g., salinity, temperature, and irradiance) on marine oil spills photodegradation; 2) analyze the significance of influencing factors and their interactions, and develop a kinetic model for the simulation of marine oil spill photodegradation. This study is anticipated to elucidate the photodegradation patterns of diverse oil spills in intricate marine environments. Furthermore, by enhancing the accuracy of marine oil spill predictions, we aim to offer a robust scientific foundation for more effective oil pollution remediation, strengthened marine environmental risk management, and the preservation of marine ecological integrity.

2. Materials and methods

2.1. Chemicals and materials

The standard compounds of *n*-alkanes (*n*-C_9 ~ *n*-C_{40}, dissolved in hexane), biomarkers (pristane and phytane) and internal standards (5-α-cholestane, *p*-terphenyl-d_{14}) were all purchased from AccuStandard (New Haven, USA). The 16-priority polycyclic aromatic hydrocarbons (16 PAHs) controlled by the United States Environmental Protection Agency and the surrogates for PAHs (naphthalene-d_8, acenaphthene-d_{10}, phenanthrene-d_{10}, chrysene-d_{12}, perylene-d_{12}) were purchased from Supelco (Bellefonte, USA). The standard compound for deuterated *n*-tetracosane (surrogate for *n*-alkanes) was purchased from Toronto Research Chemicals (Toronto, Canada).

The agents of *n*-hexane (chromatographic grade), anhydrous sodium sulfate (analytical grade) and dichloromethane (chromatographic grade) were purchased from Macklin (Shanghai, China). Column chromatography silica gel (100– 200 mesh) was purchased from Meilunbio (Dalian, China). Prior to use, the anhydrous sodium sulfate was heated at 550 °C in a muffle furnace for 4 h to remove organic residual and moisture. The silica gel was extracted with dichloromethane as the solvent using a Soxhlet extractor for 48 h, followed by drying and activation at 180 °C in a muffle furnace for 4 h.

All required glassware, such as quartz test tubes, separating funnels, and chromatographic columns, were soaked in cleaning solution, washed sequentially with tap water and ultrapure water, and then dried. The glassware was further treated in a muffle furnace at 450 °C for 4 h to eliminate interference from other organic compounds, ensuring their suitability for subsequent use.

2.2. Exposure experiments

Three types of oils: Arabian light crude oil (ALCO) from Arabia, Rapa crude oil (RCO) from Brazil and Jianghan crude oil (JCO) from China, were used to investigate the influence of oil properties on marine oil spill photodegradation. Prior to the simulation experiments, the physicochemical properties of these oils were analyzed.

To investigate the effects of environmental factors, irradiance, temperature and salinity were also considered during the photodegradation of the ALCO. For salinity, five gradient levels (0, 10, 20, 30 and 40 psu) were set based on the artificial sea water made with sodium chloride and deionized water, to simulate the salinity changes from freshwater environments to ocean seawater (Vinogradova et al., 2019). For temperature, five gradient levels (15, 20, 25, 30 and 35 °C) were set based on the variation of sea surface temperature in different oceans (Kennedy et al., 2019). Regarding irradiance, a xenon lamp (300– 1000 W) was used as the light source. The light produced by the xenon lamp, spanning wavelengths from 300 to 800 nm, closely mimics the spectrum of natural sunlight. Consequently, xenon lamps have been broadly employed in various photodegradation simulations, encompassing a range of chemicals and notably including oil spills (King et al., 2014; Shankar et al., 2015; de Bruyn et al., 2018; Liu et al., 2023; Yan et al., 2023). The relationship between the power of xenon lamp and irradiance is illustrated in **Fig. S1** in the **Supplementary Materials**. Three gradient levels, 400 W (490 μmol photons·m^{-2}·s^{-1}), 700 W (790 μmol photons·m^{-2}·s^{-1}) and 1000 W (1280 μmol photons·m^{-2}·s^{-1}), corresponding to solar radiation conditions across different latitudinal zones. Notably, the 400 W xenon lamp's irradiance is marginally below the solar noon irradiance in the northern South China Sea (nSCS) during winter. The 1000 W xenon lamp's irradiance approximates the solar noon irradiance in nSCS during the summer months (Sengupta et al., 2018).

Accordingly, three group of simulation experiments were conducted: (1) a comparative study of the three types of crude oils (ALCO, RCO and JCO) under the same conditions of temperature (25 °C), salinity (30

psu), and irradiation (1280 μmol photons·m^{-2}·s^{-1}) to investigate the influence of oil properties on marine oil spill photodegradation; (2) single-factor controlled variable experiments based on ALCO, to explore the impact of each environmental factor; (3) experiments based on an orthogonal experimental design, to analyze the significance of different influencing factors and their interactions. The specific settings of each group are listed in **Table S1** in the Supplementary Materials.

The quartz tube was placed in a photoreactor (BiLon BL-GHX-V, Fig. 1) and kept sealed during the photodegradation process. The primary components of the reactor system encompass a reaction dark chamber, a xenon lamp electrical controller, quartz reaction vessels, light sources, a cooling water circulation system, an air-cooling system, and a magnetic stirrer. The xenon lamp electrical controller allows for continuous power adjustment of the xenon lamp, ranging from 300 to 1000 W. The xenon lamp is housed within a quartz air-cooled tube, with its operating temperature regulated by the air-cooling system. The reaction vessel is a 200 mL quartz tube with an inner diameter of 3.5 cm. During the reaction, these tubes are securely placed in a sample tray inside a glass water bath. This tray is designed to accommodate up to 12 quartz tubes simultaneously. The temperature of the water bath is meticulously controlled by the cooling water circulation system, which offers precise temperature regulation ranging from -20 °C to 100 °C.

In each simulation, 1.8 g of crude oil was dissolved in 30 mL of *n*-hexane to prepare a crude oil solution with a concentration of 0.06 g·mL^{-1}. The incorporation of hexane serves to guarantee a consistent volume of crude oil is administered during each addition, thereby minimizing variations in oil quantities across disparate batches and fundamentally ensuring a uniform oil film thickness (King et al., 2014; Yang et al., 2016). This can also facilitate the isolation of photodegradation processes from other potential weathering processes, providing clearer insights into its kinetics. In a quartz tube, 60 mL of seawater and 1 mL of the crude oil solution were added. The sample tray was rotating during the photodegradation to ensure uniform irradiation for all quartz tubes. A cooling water circulation system was used to maintain the temperature in the photoreactor at the designed temperature. Previous research indicated that the photodegradation rate of marine oil spills becomes relatively slow after 5 days (Ward et al., 2018; Ward and Overton, 2020). Therefore, the simulation window of this study was set to 96 h (equivalent to 8 days under natural light conditions). After 24 h, 48 h, 72 h, and 96 h of photodegradation, samples were taken for analysis. Three parallel samples and one control group were set for each sampling time point. The control group was subjected to identical conditions as the experimental group except the irradiance (dark condition was used in this group), aiming to minimize the impact of other oil weathering processes (e.g., biodegradation).

2.3. Analytical procedures

The analytical procedures were mainly based on the method from Wang et al. (2004), with modifications on the elution program to elute all the petroleum hydrocarbons. All samples spiked with 100 μL of 200 mg·L^{-1} $C_{24}D_{50}$ (surrogate for *n*-alkanes) and 100 μL 10 mg·L^{-1} deuterated PAHs (surrogates for PAHs), were extracted with 10 mL dichloromethane (DCM) for three times.

The extracts were concentrated to 10 mL, and 1 mL which were transferred into a 3-g silica gel column (10 mm i.d.) topped with a 1-cm layer of anhydrous sodium sulfate. 20 mL DCM were used to elute the saturated and aromatic hydrocarbons. The eluate was solvent-exchanged to hexane and concentrated under nitrogen to appropriate volumes (An et al., 2023), spiked with internal standards: 50 μL 5-α-androstane (200 mg·L^{-1}) and 50 μL terphenyl-d_{14} (10 mg·L^{-1}), then adjusted to a volume of 1 mL for further instrument analysis.

The characterizations of 16 PAHs were performed on an Agilent 7890 GC system interfaced to an Agilent 5977B mass spectrometer. The compounds were separated on an Agilent HP-5 MS quartz capillary column (30 m × 0.25 mm × 0.25 μm) with the following temperature program: 60 °C for 4 min, then ramped at 40 °C·min^{-1} to 110 °C, and further ramped at 10 °C·min^{-1} to 300 °C, with a final hold for 5 min. Ultrahigh purity helium was employed as carrier gas at a flow rate of 1.5 mL·min^{-1}. The temperatures of injector, transfer line and ion source were held at 300, 280 and 230 °C, respectively. Samples were injected in splitless mode. The mass-selective detector was operated at an electron impact mode (70 eV) for selected ion monitoring (SIM) runs.

Analysis of the saturated compounds and total petroleum hydrocarbons (TPH) were performed on a Techcomp GC 7900 system equipped with a flame ionization detector (FID) and an Agilent DB-5 HT column (30 m × 0.25 mm × 0.25 μm). The carrier gas was nitrogen. (2.0 mL·min^{-1}). The injector and detector temperature were set at 300 °C and 310 °C, respectively. The temperature program used for saturated compounds was: 50 °C for 2 min, heated to 300 °C at 6 °C·min^{-1} and held for 20 min. The temperature program used for saturated compounds was: initial temperature of 40 °C, held for 2 min, then increased at a rate of 20 °C·min^{-1} to 340 °C, held for 17 min.

2.4. Quality control and quality assurance

During the experimental process, three parallel samples and one control group (dark control) were set at each sampling time point. The control group was kept under the same conditions as the experimental group, but no photodegradation was conducted, in order to eliminate the effects from evaporation and biodegradation. Additionally, procedural blanks and spiked blanks were included during the experiment. The procedural blank did not contain any indicators, while the spiked

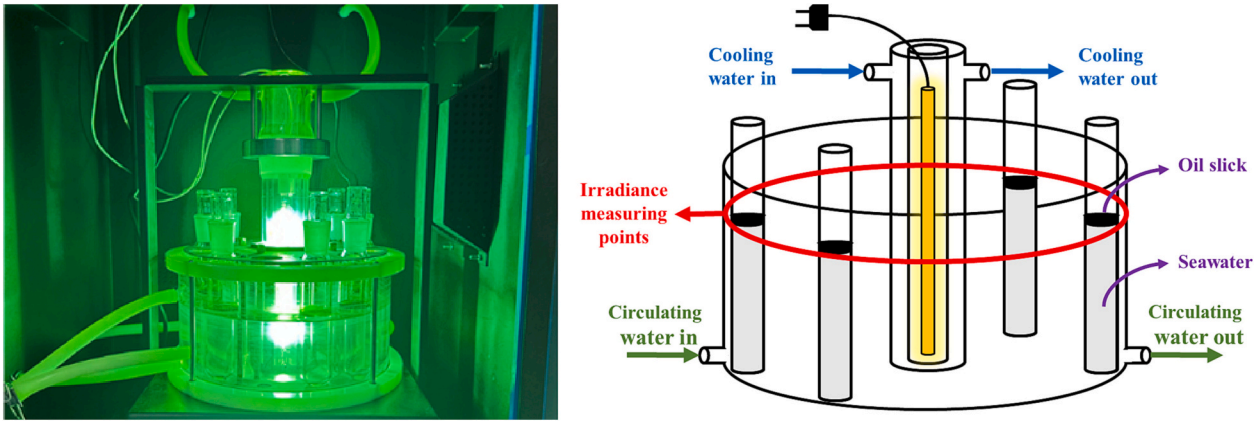

Fig. 1. Photochemical reactor for the simulation of marine oil spill photodegradation.

blank was spiked with 2 μg of PAH standard and 20 μg of *n*-alkane standard. Furthermore, in the experimental process, each sample was supplemented with 100 μL of $C_{24}D_{50}$ (200 mg·L^{-1}) and 100 μL deuterated PAHs (10 mg·L^{-1}, including naphthalene-d_8, acenaphthene-d_{10}, phenanthrene-d_{10}, chrysene-d_{12} and perylene-d_{12}) as recovery indicators. The recovery rates in all batches of experiments ranged from 60 % to 120 %, and the values obtained for procedural blanks were below the method detection limit (MLD), ensuring the validity and accuracy of the data.

2.5. Data analysis and kinetic model development

The calculation of marine oil spill photodegradation efficiency is as follows:

$$Photodegradation\ efficiency(\%) = \frac{C_0 - C_t}{C_0} \times 100 \quad (1)$$

where C_0 is the concentration of the target compound before photodegradation, and C_t is the concentration of this compound at time *t*.

Since many studies indicated that the photodegradation process of marine oil spills follows first-order reaction kinetics (Plata et al., 2008; Fu et al., 2017), this model was also considered in this study as follow:

$$\frac{dC}{dt} = -kC \quad (2)$$

where *C* is the concentration of the target compound at time *t*, *k* is the first-order reaction rate constant (day^{-1}). The integral form of this model is as follows:

$$C_t = C_0 e^{-kt} \quad (3)$$

where C_0 is the initial concentration, C_t is the concentration at time *t*. The multivariate analysis of variance (MANOVA) was then applied to identify the key factors affecting the photodegradation and to assess the interactions among these factors. Based on the Minitab® Statistical Software, a multiple regression model was developed to quantify the relationship between *k* and different key influencing factors:

$$k = f(X_1, X_2, X_3, X_1X_2, X_1X_3 \ldots\ldots) \quad (4)$$

where X_1, X_2, X_3 are the influencing factors, and X_1X_2, X_1X_3 are the interactions between different factors.

2.6. Model validation

Two scenarios were set based on the real-world condition of nSCS in summer and winter seasons, respectively. Accordingly, both laboratory and numerical simulations were conducted. By comparing the experimental and model-predicted results, the accuracy and reliability of the developed model were analyzed. The parameters for model validation are presented in Table 1 (Sengupta et al., 2018; Mao et al., 2023; Xie et al., 2023).

3. Results and discussions

3.1. Physical properties and chemical fingerprinting of the three studied oils

The properties of three crude oils are presented in **Table S2** in the Supplementary Materials. The ALCO is a light and sulfur-containing crude with low viscosity, and relatively high content of aromatics and resins. The RCO is a medium and sulfur-containing crude with low viscosity and relatively high content of aromatics and saturates. The JCO is a medium and low-sulfur crude oil with high viscosity and relatively high content of saturates. The concentrations of *n*-alkanes, biomarkers, and polycyclic aromatic hydrocarbons (PAHs) in three crude oils were listed in **Figs. S2** and **S3** in the **Supplementary Materials**, indicating the differences in the distribution of *n*-alkanes and PAHs among these oils. The ALCO mainly consists of *n*-alkanes ranging from *n*-nonane (*n*-C_9) to *n*-hexadecane (*n*-C_{16}). The PAHs in the ALCO are dominant by naphthalene (Nap), acenaphthene (Acy), fluorine (Flu), phenanthrene (Phe) and chrysene (Chr). The JCO is characterized by *n*-alkanes mainly between *n*-tetradecane (*n*-C_{14}) and *n*-tetracosane (*n*-C_{24}), and PAHs primarily composed of Nap, Phe, benzo[*a*]anthracene (BaA), Chr and benzo[*a*]pyrene (BaP). It is worth noting that the JCO appears a lower ratio of pristane/phytane compared to the other two oils. The RCO appears lower abundances of *n*-alkanes and PAHs, with *n*-alkanes mainly concentrated in lower carbon numbers (*n*-C_9 ~ *n*-C_{24}), and a richer composition of PAHs. In general, three oils appear significant differences in their properties, and can be used to investigate the effect of oil properties on photodegradation.

3.2. Effect of oil properties

Besides setting up the dark control group, the ratios of *n*-C_{17}/Pristane and *n*-C_{18}/Phytane were also monitored during the laboratory simulation to avoid the interference from other oil weathering processes during the photodegradation (**Fig. S4** in the **Supplementary Materials)**. Over the 4-day simulation, the relative standard deviations of these two ratios were all below 10 % for all the oils, indicating insignificant biodegradation occurred during the simulation experiment.

The concentrations of total *n*-alkanes, total PAHs and TPHs in three oils after photodegradation are presented in Fig. 2. Significant decreases in *n*-alkanes, PAHs and TPHs concentrations were observed after the photodegradation, indicating the occurrence of photodegradation in all the oils. After 4 days of photodegradation, the concentrations of total PAHs in ALCO, LCO and JCO decreased by 89.2 %, 89.9 % and 81.8 %, respectively. In addition, the concentrations of total *n*-alkanes in ALCO, LCO and JCO decreased by 22.2 %, 11.8 % and 9.5 %, respectively. The photodegradation efficiency of total PAHs was significantly higher than that of total *n*-alkanes, which is consistent with the previous research findings (Bacosa et al., 2015; Yang et al., 2016). Many compounds in PAHs are photosensitive and capable of directly absorbing photons. Comparatively, *n*-alkanes can only undergo reactions through indirect photodegradation pathways, leading to a lower photodegradation efficiency than PAHs (D'Auria et al., 2009).

After 4 days of photodegradation, the TPHs concentrations in ALCO, LCO and JCO decreased by 22.3 %, 15.9 %, and 12.6 %, respectively. Previous research has indicated that factors such as viscosity, aromatic content, sulfur content, and asphaltene content could influence the efficiency of marine oil spill photodegradation (Chacón-Patiño et al., 2017; Niles et al., 2020; Yang et al., 2022). To further investigate the impact of oil properties on photodegradation, Pearson correlation analysis was conducted between the degradation efficiency and relevant physicochemical parameters. The corresponding results are listed in **Table S3** in the **Supplementary Materials**. Asphaltene content appeared the most significant correlation with the degradation efficiency ($R = 0.997$, $p < 0.05$) among all seven indicators. Unlike many aromatic compounds that can only absorb ultraviolet light, asphaltene can absorb both ultraviolet and visible lights. Additionally, significant correlation was also observed between oil density and photodegradation efficiency ($R = -0.993$, $p = 0.075$), suggesting that oil density could be another important factor influencing photodegradation. Usually, oils with higher density tend to have a higher proportion of heavy compounds. The compounds in the heavy fraction are relatively more

Table 1
Settings for model validation.

Scenario	Temperature °C	Salinity psu	Irradiance μmol photons·m^{-2}·s^{-1}
nSCS summer	28.5	33	1000
nSCS winter	17.5	34	620

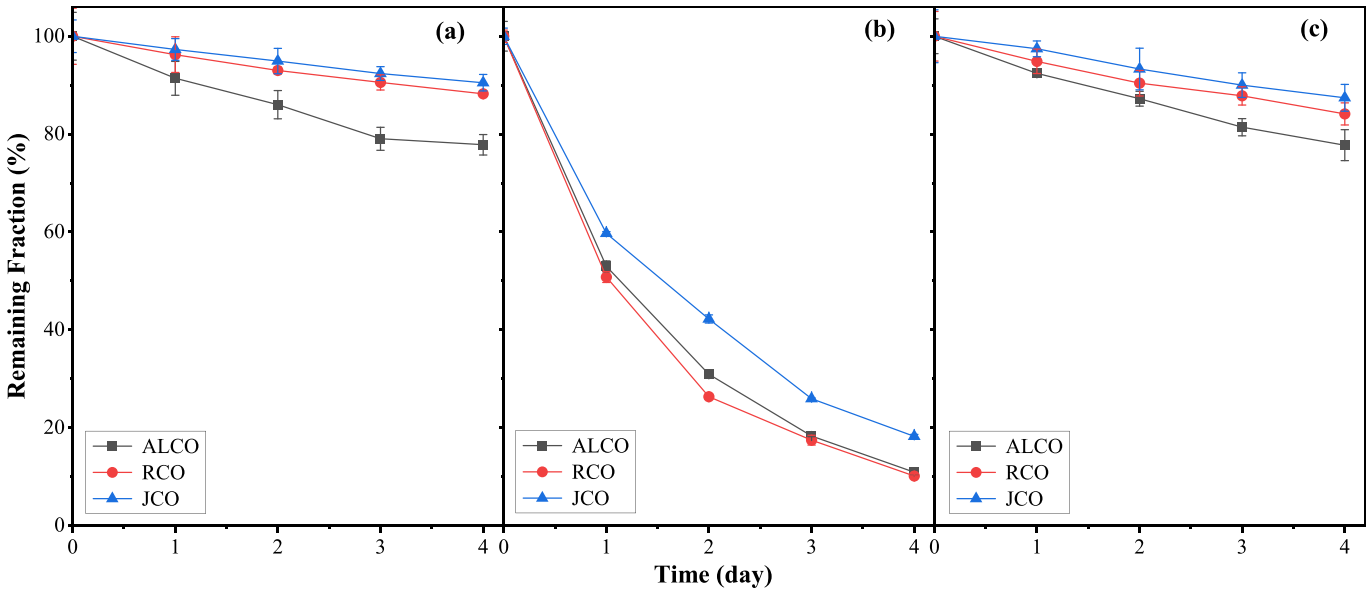

Fig. 2. Concentration changes of (a) total *n*-alkanes (C_9-C_{35}), (b) total PAHs and (c) TPHs in three crude oils during photodegradation.

resistant to photodegradation compared to those in the light fraction (Cook et al., 2020). Furthermore, oils with higher density form thicker oil slicks, reducing the efficiency of oil photodegradation (Guo et al., 2020). Additionally, denser oils are more prone to sinking, limiting their exposure to light (Ye et al., 2020). Currently, the research on the effects of asphaltene content and density on oil photodegradation is still limited. Further research is needed for the mechanisms of visible light-driven oil photodegradation. It is noteworthy that the inclusion of hexane not only facilitates a focused investigation into the kinetics of photodegradation but also mitigates the impact arising from variations in oil thickness, potentially leading to an underestimation of the influence exerted by oil viscosity. Given that both oil thickness and viscosity play crucial roles in oil weathering processes, a detailed exploration of their effects on the interplay between photodegradation and other weathering mechanisms will necessitate further investigation, both in subsequent tank experiments and field tests.

Significant decrease was observed for low-molecular-weight *n*-alkanes (*n*-C_9 ~ *n*-C_{15}) and medium-molecular-weight *n*-alkanes (*n*-C_{16} ~ *n*-C_{23}) in all oils (Fig. 3), with degradation efficiencies exceeding 10 %. Comparatively, high-molecular-weight *n*-alkanes (*n*-C_{24} ~ *n*-C_{35}) appeared insignificant changes. The efficiency of *n*-alkanes in all three crude oils exhibited a decreasing trend with increasing molecular weight. The high-molecular-weight *n*-alkanes appeared resistance to photodegradation due to steric hindrance, which was consistent with the findings from previous studies (Heath et al., 1997; Yang et al., 2022).

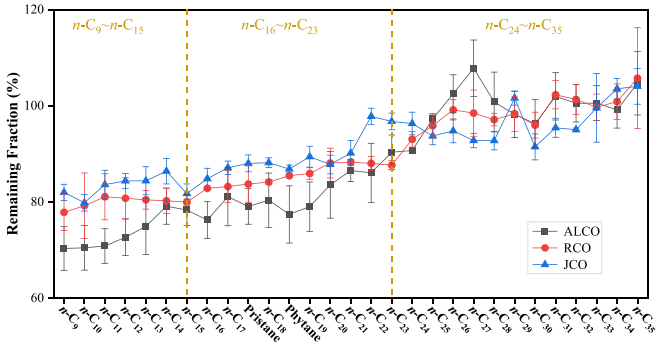

Fig. 3. Remaining fraction of *n*-alkanes in three crude oils after 4-day photodegradation.

The efficiency of pristane and phytane was slightly higher than that of *n*-heptadecane and *n*-octadecane, indicating that branched alkanes were more susceptible to photodegradation compared to *n*-alkanes (D'Auria et al., 2008).

In contrast to the pattern observed for *n*-alkanes, the photodegradation efficiency of PAHs in three oils displayed different trends with the number of rings (Fig. 4). High-ring PAHs in ALCO appeared higher degradation efficiency, while the efficiency of low-ring PAHs was generally higher in LCO. The efficiency of PAHs in JCO showed insignificant correlation with the number of rings. Theoretically, high-ring PAHs have higher spectral overlap with solar spectra compared to low-ring PAHs, allowing them to absorb a greater number of photons during the photodegradation. Usually, the quantity of absorbed photons is significantly correlated with the photodegradation efficiency. After absorbing photons, PAHs can be excited to singlet or triplet states, and subsequently transfer energy to ground-state molecular oxygen ($^3O_2$), generating ROS (e.g., singlet oxygen ($^1O_2$)) easily. Stout et al. (2016) found that high-ring PAHs appeared more significant concentration losses than low-ring PAHs in the floating and stranded oil samples from the Deepwater Horizon oil spill. Nevertheless, the results from this study suggested that the other properties of the crude oil can influence the photodegradation of PAHs in spilled oil. Previous studies have indicated that the water solubility of photodegraded products increased and could be further photodegraded, affecting the photodegradation of the parent PAHs (Zito et al., 2014). The photodegradation patterns of PAHs among different types of crude oil still need to be further investigated.

3.3. *Effect of environmental factors*

3.3.1. *Salinity*

Fig. 5 indicates the photodegradation of total *n*-alkanes, total PAHs and TPHs under different salinity conditions. The degradation of individual compounds can be found in **Figs. S5a** and **S6a** in the **Supplementary Materials**. After 4-day photodegradation, the concentrations of total *n*-alkanes, total PAHs and TPHs appeared significant decreases under all five salinity conditions. Nevertheless, no statistical difference was observed in the concentration changes among the five salinity treatment groups ($p > 0.05$). In previous studies, the effect of chloride ions (Cl^-) on the photodegradation of organic compounds remains inconclusive. Some studies have reported that under high salinity conditions, Cl^- can accelerate the photodegradation of organic compounds by promoting the formation of $^1O_2$ and ·OH radicals (Ge et al., 2009). In

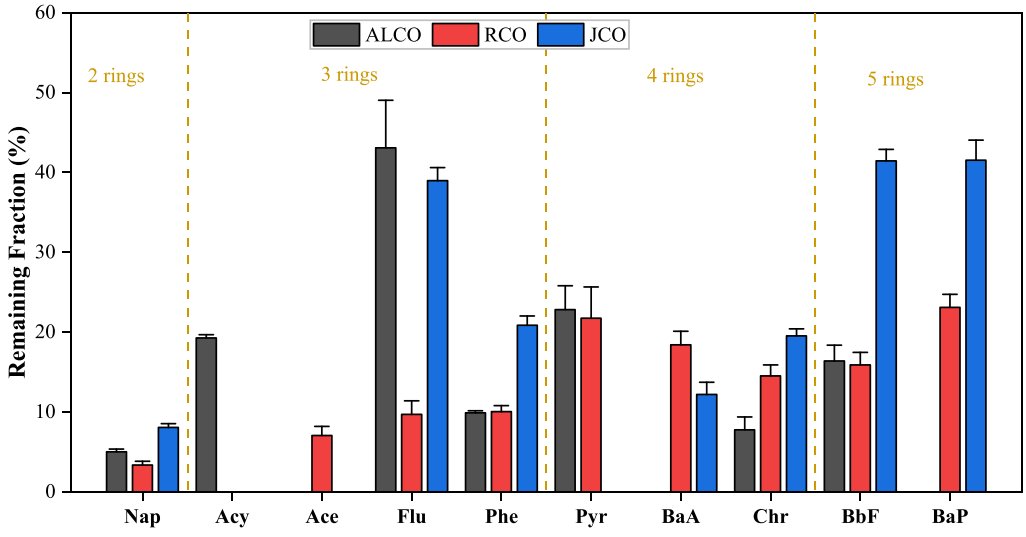

Fig. 4. Remaining fraction of PAHs in three crude oils after 4-day photodegradation.

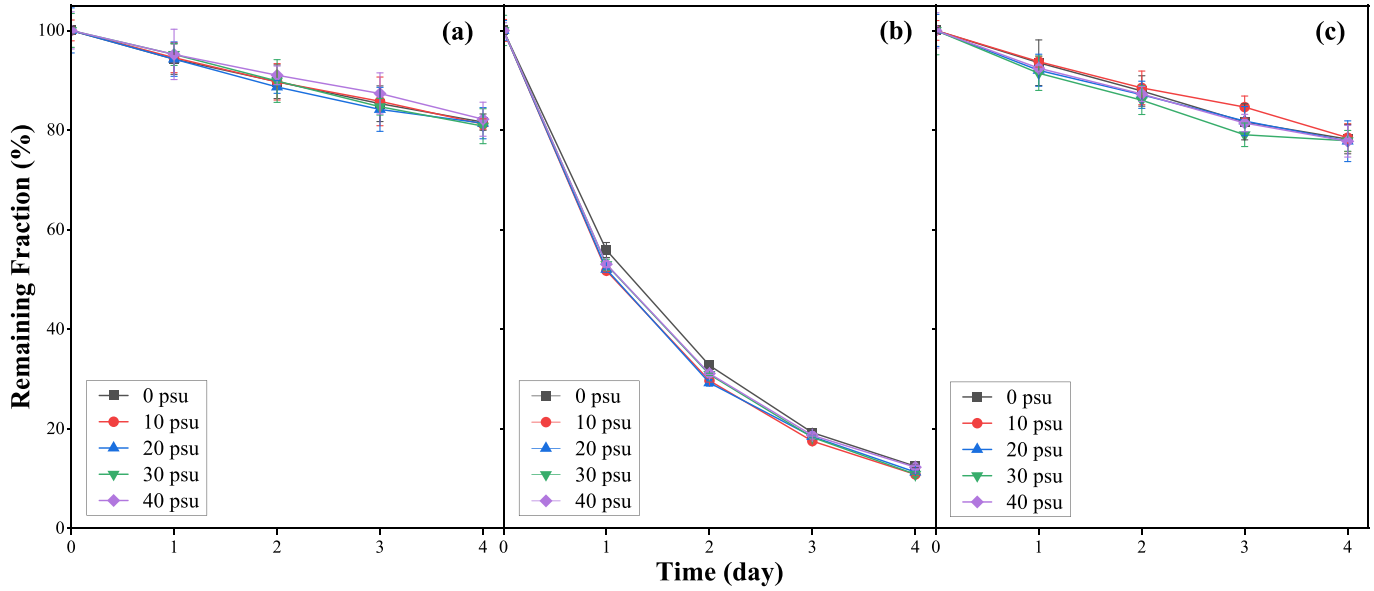

Fig. 5. Changes of (a) total *n*-alkanes (*n*-C_9 ~ *n*-C_{35}), (b) total PAHs and (c) total petroleum hydrocarbons after photodegradation under different salinity conditions.

contrast, other studies have yielded opposite results, as Kong and Ferry (2004) found that Cl^- can quench $^1O_2$ and consequently inhibit the photodegradation rate of Chr.

In the photodegradation of marine oil spills, the generation of free radicals is a crucial step in the indirect photodegradation. Previous research has found that under illumination, chlorine radicals (Cl· and Cl_2·-) could be produced in seawater and participate in the photodegradation of pollutants. Nevertheless, the experimental results in this study suggested that the generation of chlorine radicals did not significantly affect the photodegradation of spilled oil. Possible reasons for this discrepancy are as follows: 1) The spilled oil primarily exists as a floating oil slick, leading to insufficient contact of petroleum compounds and the Cl^- in water column (García-Martínez et al., 2006); 2) The quantity of chlorine radicals produced in this study may be insufficient to promote indirect photodegradation, and the free radicals in the indirect photodegradation are mainly generated by light-absorbing species in the spilled oil, such as PAHs and asphaltene.

3.3.2. *Temperature*

To avoid the effect of oil evaporation, this study compared the concentration changes of various oil compounds under different temperature conditions in the dark control group. It was observed that the concentrations of oil compounds decreased on average by 0.75 ± 2.95 % under different temperature conditions, and were not statistically significant ($p > 0.05$). These results indicate that insignificant evaporation occurred during all simulations.

Fig. S7 in the **Supplementary Materials** illustrates the changes of oil slick during photodegradation at 35 °C. Throughout the process, the color of the oil slick gradually lightened, and with noticeable cracking, indicating a significant degradation of the spilled oil. The changes of total *n*-alkanes, total PAHs, and TPHs under different temperature conditions are shown in Fig. 6. Specific degradation data for individual compounds are provided in **Figs. S5b** and **S6b** in the **Supplementary Materials**. The photodegradation efficiencies of *n*-alkanes, PAHs, and TPHs appeared significant differences ($p < 0.05$) among different temperature conditions, indicating that temperature is a critical factor influencing the photodegradation. Furthermore, significantly positive

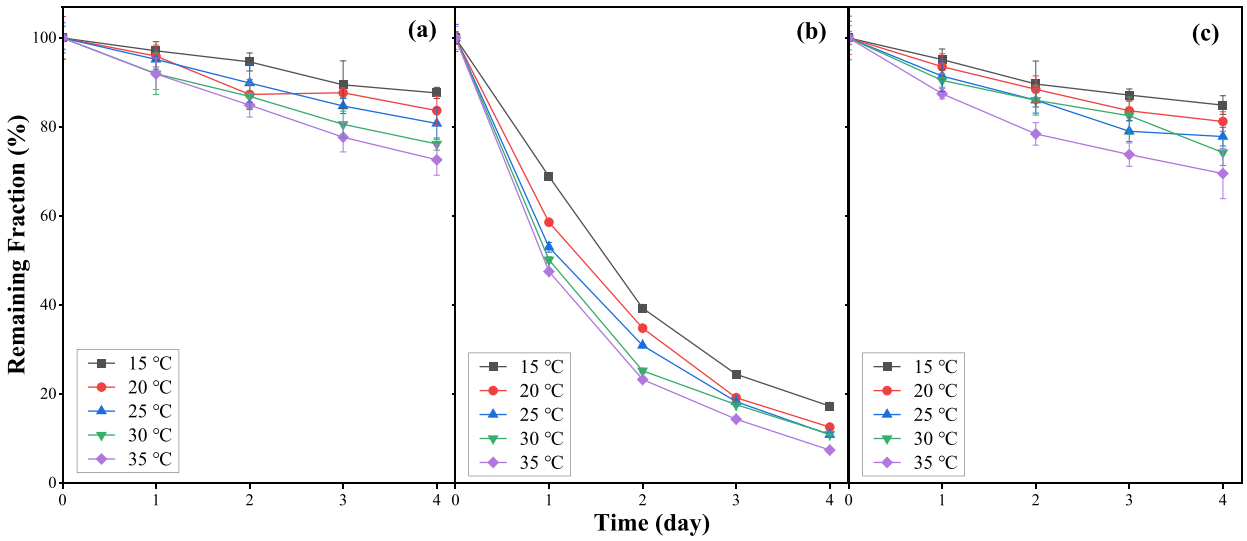

Fig. 6. Changes of (a) total *n*-alkanes (*n*-C_9 ~ *n*-C_{35}), (b) total PAHs and (c) TPHs after photodegradation under different temperature conditions.

correlation was observed between photodegradation efficiency and temperature.

In photochemical reactions, activation molecules mainly arise from molecular absorption of photons. Therefore, the number of activation molecules is less dependent on temperature. Jing et al. (2014) indicated that the influence of temperature on the photodegradation rate of naphthalene is less significant than the impact of irradiance. Nevertheless, this study found significant effect of temperature on the photodegradation efficiency of spilled oil, for both *n*-alkane and PAH components. This indicates that the photochemical reaction mechanisms in complex spilled oils may differ from those observed in single compounds (e.g., naphthalene) (Chen et al., 2016; White et al., 2016). The ALCO contains 27.34 % saturated and 40.40 % aromatic hydrocarbons, both of which can undergo reactions through the indirect photodegradation pathway. Several field observations after the Deepwater Horizon oil spill have demonstrated the significance of the indirect photodegradation (Aeppli et al., 2018; Niles et al., 2019). An essential step in the indirect photodegradation process involves the collision between petroleum hydrocarbon molecules and reactive oxygen species (ROS). The increase in temperature enhances the molecular diffusion and collision strength between petroleum hydrocarbon molecules and ROS, accelerating the formation and dissociation of charge-transfer complexes. Furthermore, elevated temperatures can increase the solubility of petroleum hydrocarbons in seawater (Saeed et al., 2011).

The concentration of *n*-C_{23} ~ *n*-C_{29} appeared slight increase on the third day after photodegradation at 20 °C (**Fig. S8** in the **Supplementary Materials)**. The possible reason could be: 1) the photolytic ring-opening reactions of highly alkylated aromatics, resulting in the formation of *n*-alkanes; or 2) the photolytic decarboxylation of alkanoic acids, leading to the generation of *n*-alkanes (Wang et al., 2020). Similar findings were reported in the studies by Dutta and Harayama (2000), where a noticeable increase in the concentration of certain *n*-alkanes in crude oil was observed after photodegradation. Thus, besides the formation of aldehydes, acids and other oxygenated hydrocarbon derivatives, photodegradation can also lead to the generation of *n*-alkanes.

Fig. 7 compares the photodegradation of several *n*-alkanes (i.e., *n*-nonane (*n*-C_9), *n*-decane (*n*-C_{10}), *n*-undecane (*n*-C_{11})) and PAHs (i.e., Acy, Phe, and Chr) at the temperatures of 15 °C and 35 °C. With a 20 °C increase in temperature, the photodegradation efficiencies of *n*-C_9, *n*-C_{10} and *n*-C_{11} increased by 18 %, 16 %, and 14 %, respectively. The degradation efficiencies of Acy, Phe, and Chr increased by 8 %, 11 %, and 5 %, respectively. The rise in temperature presented more

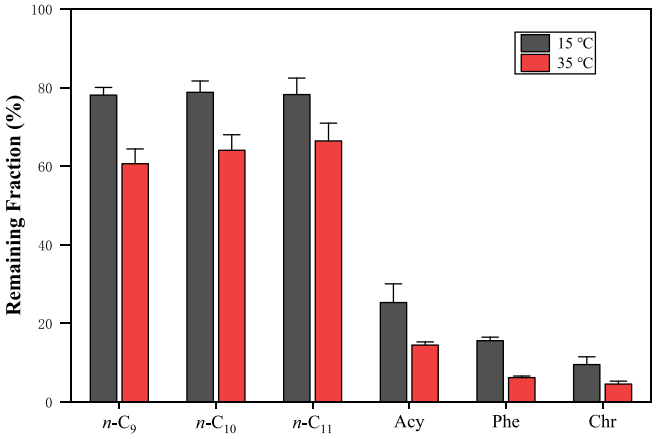

Fig. 7. Remaining fraction of several *n*-alkanes and PAHs in 15 °C and 35 °C after 4-day photodegradation.

significant effect on the photodegradation of *n*-alkanes compared to PAHs. Previous studies have indicated that compounds with higher activation energies for photodegradation exhibit a greater sensitivity of photodegradation rates to environmental temperatures (Kang et al., 2019). Similarly, this study found that *n*-alkanes appeared a higher sensitivity to temperatures than PAHs, suggesting a higher activation energy required for the photochemical reactions of *n*-alkanes.

3.3.3. *Irradiance*

Fig. 8 presents the photodegradation of total *n*-alkanes, total PAHs, and TPHs under different irradiance conditions. The specific degradation profiles of individual compounds can be found in **Figs. S5c** and **S6c** in the **Supplementary Materials**. The photodegradation efficiency of *n*-alkanes, PAHs, TPHs appeared significant differences under different irradiances ($p < 0.05$). Increasing irradiance resulted in higher efficiency for all components, showing a clear positive correlation between photodegradation efficiency and irradiance.

Eqs. (5) to (8) represent the photodegradation pathways for PAHs and *n*-alkanes. The increase in irradiance provides more photons, supplying energy for additional photodegradation reactions. In normal conditions, petroleum hydrocarbons remain in a stable ground state. Upon photon absorption, they can be excited to higher-energy and less stable excited states, leading to reactions (Cai et al., 2017). Higher

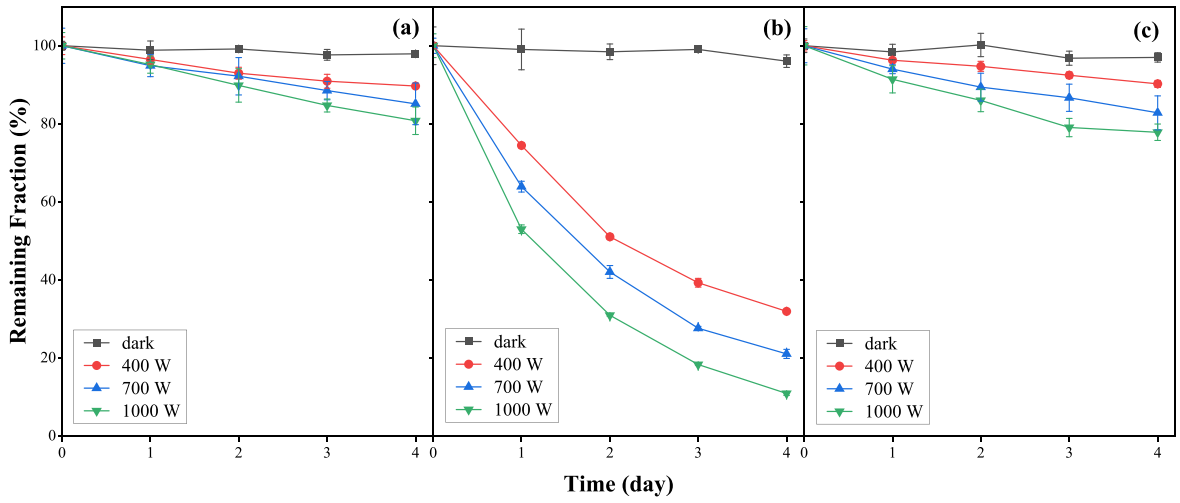

Fig. 8. Changes of (a) total alkanes (n-C_9 ~ n-C_{35}), (b) total PAHs and (c) TPHs under different irradiance conditions.

irradiance allows more molecules to reach the excited state and participate in photodegradation. Furthermore, both direct and indirect photodegradation pathways rely on light-absorbing substances to drive the reactions. Changes in irradiance not only affect the efficiency of exciting aromatic components to their excited states but also influence the generation of ROS (Zhang et al., 2011). As a result, irradiance plays a crucial role in the photodegradation process of marine oil spills.

$$PAH \xrightarrow{h\nu} PAH^{+} \rightarrow Products \tag{5}$$

$$PAH \xrightarrow{h\nu} {}^{1}[PAH]^{*} \xrightarrow{{}^{3}O_2} PAH^{+} + \cdot O_2^{-} \rightarrow Products \tag{6}$$

$$PAH \xrightarrow{h\nu} {}^{1}[PAH]^{*} \xrightarrow{{}^{3}O_2 \text{ or } {}^{1}O_2^{*}} {}^{3}[PAH]^{*} + {}^{1}O_2^{*} \xrightarrow{{}^{3}O_2} Products \tag{7}$$

$$Photosensitizer(PAH) \xrightarrow{h\nu} ROS\left(\cdot OH, {}^{1}O_2, \cdot OOR\right) + Alkane \rightarrow Products \tag{8}$$

Compared to n-alkanes, PAHs appeared higher sensitivity to irradiance. Fig. 9 illustrates the differences in photodegradation efficiency for several components under irradiance with 400 W (490 μmol photons•m^{-2}•s^{-1}) and 1000 W (1280 μmol photons•m^{-2}•s^{-1}) xenon lamp. With the rise in irradiance, the degradation efficiency of PAHs increased more significantly than which of n-alkanes. During the photodegradation, there are variations in the degradation pathways between saturated and aromatic hydrocarbons. Aromatic hydrocarbons have the ability to directly absorb photons, allowing them to be excited to an excited state and proceed direct photodegradation. Comparatively, saturated hydrocarbon cannot directly absorb photons and only participate in indirect photodegradation through reactions with ROS that generated by photosensitizers (e.g., PAHs, humic substances and anthraquinone) after absorption of photons. Thus, saturated hydrocarbons generally have lower photodegradation rates compared to aromatic hydrocarbons (O'Connor et al., 2019; Zito et al., 2020). Since most PAHs possess the capability of directly absorbing photons, the aromatic hydrocarbons appear higher sensitivity irradiance compared to n-alkanes. Consequently, their photodegradation efficiency is more significantly affected by irradiance.

3.4. Kinetic analysis and photodegradation model development

The first-order kinetic model was applied to fit the concentration changes of n-alkanes and PAHs in three crude oils under different environmental conditions. The first-order rate constants (k) are presented in **Tables S4** to **S8** in the **Supplementary Materials**. The results demonstrate that the concentration changes of most components in three oils were well-fitted by the first-order kinetic model ($R^2 > 0.95$, $p < 0.05$). The k values for PAHs were ranging from 0.2044 to 0.8148 day^{-1}, while the ones for n-alkanes were ranging from 0.0068 to 0.1002

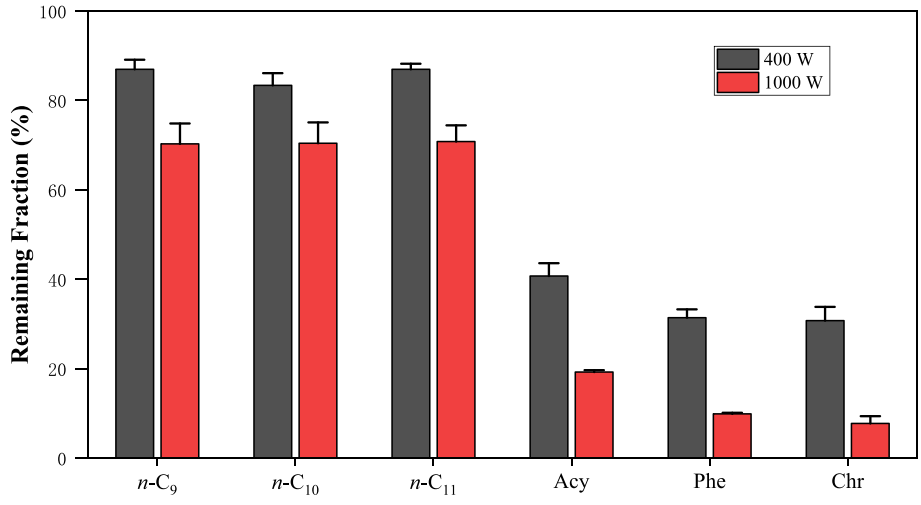

Fig. 9. Remaining fraction of several n-alkanes and PAHs after 4 days of irradiation with 400 W and 1000 W xenon lamp.

day^{-1}. The rate constants for PAHs are significantly higher than which for *n*-alkanes, complying with the previous findings in this study, as well as the finding from Bacosa et al. (2015).

To facilitate the study of the overall transport and fate of marine oil, this research conducted a kinetic analysis for the changes of TPHs concentration during photodegradation. The fittings of TPHs photodegradation for different oils and under different environmental conditions were illustrated in **Figs. S9** and **S10** in the **Supplementary Materials**. The results indicate that the first-order kinetic model could satisfactorily fit the changes of TPHs concentration during photodegradation in all treatment groups ($R^2 > 0.95$, $p < 0.05$), demonstrating that photodegradation of TPHs in three oils all follows first-order kinetic behavior under different environmental conditions. The *k* values for ALCO, LCO and JCO were 0.0645 day^{-1}, 0.0423 day^{-1} and 0.0348 day^{-1}, respectively.

To investigate the significance of the factors and their interactions, MANOVA was conducted. The results of the analyses are listed in **Table S9** in the **Supplementary Materials**, where the factors and interactions with *p*-values <0.05 are considered to have a significant effect on the photodegradation. It is worth noting that the third-order term was not considered in the analysis due to its insignificant effect. In terms of the main factors, temperature and irradiance appeared significant effects, while salinity did not show a significant effect on the photodegradation. Furthermore, the interaction between temperature and irradiance also presented a significant effect to the degradation.

Based on the results from MANOVA, this study selected irradiance and temperature as independent variables and the first-order reaction rate constant (*k*) of TPHs photodegradation as the dependent variable. The regression model was developed according to Eq. (4), based on the Minitab® 21.1 software. After performing a natural logarithm transformation on the constant *k*, the regression model is generated as follows:

$$lnk = 0.022T + 0.762I + 0.013T \times I - 4.702 \tag{9}$$

where *T* is temperature (°C), and *I* is irradiance (mmol photons•m^{-2}•s^{-1}). The corresponding response surface of the model is illustrated in **Fig. S9** in the **Supplementary Materials**. An R^2 value of 0.9731 was obtained for the regression, indicating a good fit of the model. The calculated rate constant *k* was then applied to Eq. (3) for the simulation of marine oil spill photodegradation.

Based on the Pareto chart analysis, the significances of factors (temperature, irradiance, and their interaction) were quantified. The result of the analysis is presented in **Fig. S10** in the **Supplementary Materials**. The order of significance for the three factors is: irradiance > temperature > irradiance-temperature interaction. This suggests that irradiance is the key factor affecting the marine oil spill photodegradation. Similar conclusions were drawn by Jing et al. (2014) in their study of naphthalene photodegradation in oily wastewater, where irradiance was identified as the critical factor influencing naphthalene photodegradation. The analysis also indicates that temperature has a slightly lower but still significant impact on the photodegradation. Increasing temperature enhances the diffusion and collision between petroleum hydrocarbon molecules and ROS, accelerating the formation and dissociation of charge-transfer complexes. Furthermore, the irradiance-temperature interaction also has a noticeable effect. The increase in irradiance elevates the average molecular kinetic energy and internal energy, leading to higher temperatures and promoting the photodegradation of oil spills.

The developed model was validated based on the real-world conditions of nSCS, with summer and winter scenarios (Table 1). The comparison between the laboratory simulation and numerical model prediction is presented in Fig. 10. In general, the developed marine oil spill photodegradation kinetic model was able to provide satisfactory prediction to the changes in TPHs concentration in both scenarios.

The accuracy of the model was further evaluated based on the Nash-

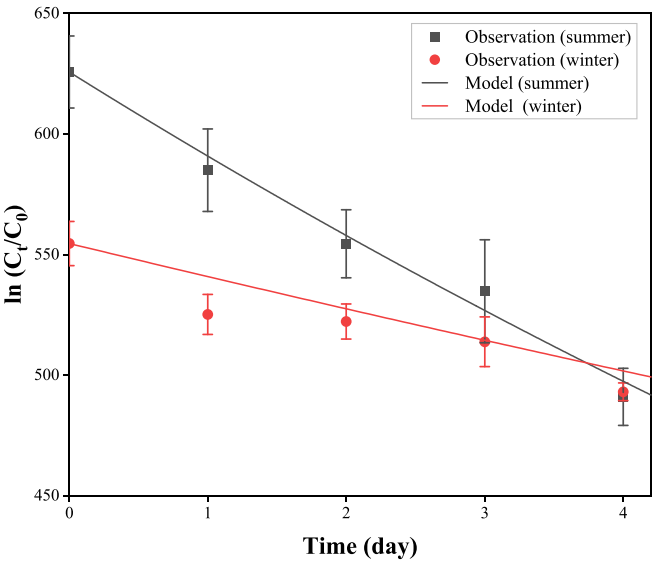

Fig. 10. Change of TPHs in the scenario of nSCS (a) summer and (b) winter.

Sutcliffe model efficiency coefficient (NSE), root mean square error (RMSE), and the ratio of RMSE to the standard deviation of observed values (RSR) as follows (Moriasi et al., 2007):

$$NSE = 1 - \frac{\sum_{i=1}^{n}(O_i - P_i)^2}{\sum_{i=1}^{n}(O_i - \overline{O})^2} \tag{10}$$

$$RMSE = \sqrt{\frac{1}{n}\sum_{i=1}^{n}(O_i - P_i)^2} \tag{11}$$

$$RSR = \frac{RMSE}{\sqrt{\frac{1}{n}\sum_{i=1}^{n}(O_i - \overline{O})^2}} = \frac{\sqrt{\frac{1}{n}\sum_{i=1}^{n}(O_i - P_i)^2}}{\sqrt{\frac{1}{n}\sum_{i=1}^{n}(O_i - \overline{O})^2}} \tag{12}$$

where: O_i is the observed values, P_i is the model-predicted values and $\overline{O}$ is the mean value of the observed data. Corresponding results are listed in Table 2. The developed model appeared high accuracy (NSE = 0.974) and high reliability (RSR = 0.180) in the prediction of marine oil spill photodegradation in the nSCS summer scenario. In addition, the model's performance was slightly lower in the nSCS winter scenario, but it still maintained a high level of accuracy (NSE = 0.758) and acceptable reliability (RSR = 0.744).

4. Conclusion

This study comprehensively analyzed the photodegradation dynamics of marine oil spills, unearthing the intricate interplay between oil properties and multifarious environmental determinants. The results indicated that asphaltene fraction played a crucial and positive role to the marine oil spill photodegradation. In addition, the density of the oil could be an important factor with negative effects. For environmental conditions, the impact of salinity on the degradation was insignificant and required further investigation. Comparatively, elevated

Table 2
Model validation results.

Statistics	nSCS summer	nSCS winter
NSE	0.974	0.758
RMSE	6.137	9.346
RSR	0.180	0.744

temperatures and increased irradiance significantly promoted the photodegradation. Compared to PAHs, *n*-alkanes appeared lower irradiance sensitivity and higher temperature sensitivity in their photodegradation efficiency. In addition, the degradation efficiency of *n*-alkane nagetively correlated with its carbon numbers.

The first-order kinetic model could adequately fit the photodegradation of *n*-alkanes, PAHs, and TPHs for different oils under varied environmental conditions, with rate constants of 0.0645 day^{-1}, 0.0423 day^{-1} and 0.0348 day^{-1} for the Arabian light crude oil, Rapa crude oil and Jianghan crude oil, respectively. Accordingly, a novel model was developed to determine the rate constant for marine oil spill photodegradation under different environmental conditions and their interactions. The model indicated that irradiance, temperature and their interaction were key affecting factors, with the significance of irradiance > temperature > irradiance-temperature interaction. Finally, the validation of the model had demonstrated its applicability the simulation of marine oil spill photodegradation. In general, the findings of this study provide a scientific basis for the prevention and remediation of oil pollution, the improvement of marine environmental risk management, and the preservation of marine ecological security.

While this study establishes a foundational framework for comprehending the kinetics of oil spill photodegradation, it's imperative to acknowledge the inherent simplifications and controlled conditions underpinning its development. Future endeavors will rigorously evaluate and refine the model to incorporate more nuanced factors, including light source variability, viscosity, and influences from oil slick dynamics, as well as exploring interactions between photodegradation and other oil weathering processes. Both tank experiments and field tests will be undertaken to enhance the model further, taking into additional consideration the effects of wind and wave-induced turbulent mixing.

CRediT authorship contribution statement

Pu Li: Conceptualization, Methodology, Investigation, Formal analysis, Validation, Writing – original draft, Visualization, Funding acquisition. **Zhenhua Lu:** Methodology, Investigation, Data curation, Formal analysis, Writing – review & editing. **Shichun Zou:** Writing – review & editing, Supervision, Funding acquisition. **Lihua Yang:** Investigation, Writing – review & editing, Supervision, Project administration, Funding acquisition.

Declaration of competing interest

The authors declare that they have no known competing financial interests or personal relationships that could have appeared to influence the work reported in this paper.

Data availability

No data was used for the research described in the article.

Acknowledgement

This research was funded by the Guangdong Basic and Applied Basic Research Foundation – General Program (project numbers: 2023A1515012123) and the Guangdong Science and Technology Department - Key Area Research and Development Program of Guangdong Province (project numbers: 2020B1111350003).

Appendix A. Supplementary data

Supplementary data to this article can be found online at https://doi.org/10.1016/j.marpolbul.2023.115729.

References

Aeppli, C., 2022. Recent advance in understanding photooxidation of hydrocarbons after oil spills. Curr. Opin. Chem. Eng. 36, 100763.
Aeppli, C., Swarthout, R.F., O Neil, G.W., Katz, S.D., Nabi, D., Ward, C.P., Nelson, R.K., Sharpless, C.M., Reddy, C.M., 2018. How persistent and bioavailable are oxygenated Deepwater Horizon oil transformation products? Environ. Sci. Technol. 52 (13), 7250–7258.
Aeppli, C., Mitchell, D.A., Keyes, P., Beirne, E.C., McFarlin, K.M., Roman-Hubers, A.T., Rusyn, I., Prince, R.C., Zhao, L., Parkerton, T.F., Nedwed, T., 2022. Oil irradiation experiments document changes in oil properties, molecular composition, and dispersant effectiveness associated with oil photo-oxidation. Environ. Sci. Technol. 56 (12), 7789–7799.
An, C.X., He, Y.T., Ran, Z., Li, R., Liu, S.H., 2023. Comparison study of the determination results of petroleum hydrocarbons by infrared spectrophotometry and gas chromatography (C10 ~ C40). Appl. Chem. Ind. 52 (8), 2423–2426.
Arekhi, M., Terry, L.G., Clement, T.P., 2023. Characterizing the efficiency of low-cost LED lights for conducting laboratory studies to investigate polycyclic aromatic hydrocarbon photodegradation processes. Environ. Res. 217, 114951.
Bacosa, H.P., Erdner, D.L., Liu, Z., 2015. Differentiating the roles of photooxidation and biodegradation in the weathering of Light Louisiana Sweet crude oil in surface water from the Deepwater Horizon site. Mar. Pollut. Bull. 95 (1), 265–272.
de Bruyn, W., Chang, D., Bui, T., Hok, S., Clark, C., 2018. Photochemical degradation of oil products in seawater monitored by 3D excitation emission matrix (EEM) fluorescence spectroscopy: implications for coloured dissolved organic matter (CDOM) studies. Environ. Sci. Pollut. Res. Int. 25 (34), 34777–34787.
Cai, Z., Liu, W., Fu, J., O'Reilly, S.E., Zhao, D., 2017. Effects of oil dispersants on photodegradation of parent and alkylated anthracene in seawater. Environ. Pollut. 229, 272–280.
Chen, H., Hou, A., Corilo, Y.E., Lin, Q., Lu, J., Mendelssohn, I.A., Zhang, R., Rodgers, R. P., McKenna, A.M., 2016. 4 Years after the Deepwater Horizon spill: molecular transformation of Macondo well oil in Louisiana salt marsh sediments revealed by FT-ICR mass spectrometry. Environ. Sci. Technol. 50 (17), 9061–9069.
Cook, L.L., Drollette, B.D., Edwards, M.R., Benton, L.D., Boehm, P.D., 2020. A data-driven framework for defining stages of oil weathering. Mar. Pollut. Bull. 154, 111091.
D'Auria, M., Racioppi, R., Velluzzi, V., 2008. Photodegradation of crude oil: liquid injection and headspace solid-phase microextraction for crude oil analysis by gas chromatography with mass spectrometer detector. J. Chromatogr. Sci. 46 (4), 339–344.
D'Auria, M., Emanuele, L., Racioppi, R., Velluzzi, V., 2009. Photochemical degradation of crude oil: comparison between direct irradiation, photocatalysis, and photocatalysis on zeolite. J. Hazard. Mater. 164 (1), 32–38.
Dutta, T.K., Harayama, S., 2000. Fate of crude oil by the combination of photooxidation and biodegradation. Environ. Sci. Technol. 34 (8), 1500–1505.
Fu, J., Gong, Y., Cai, Z., O'Reilly, S.E., Zhao, D., 2017. Mechanistic investigation into sunlight-facilitated photodegradation of pyrene in seawater with oil dispersants. Mar. Pollut. Bull. 114 (2), 751–758.
García-Martínez, M.J., Da Riva, I., Canoira, L., Llamas, J.F., Alcántara, R., Gallego, J.L.R., 2006. Photodegradation of polycyclic aromatic hydrocarbons in fossil fuels catalysed by supported TiO_2. Appl. Catal. B Environ. 67 (3–4), 279–289.
Ge, L., Chen, J., Qiao, X., Lin, J., Cai, X., 2009. Light-source-dependent effects of main water constituents on photodegradation of phenicol antibiotics: mechanism and kinetics. Environ. Sci. Technol. 43 (9), 3101–3107.
Guo, G., Liu, B., Liu, C., 2020. Thermal infrared spectral characteristics of bunker fuel oil to determine oil-film thickness and API. J. Mar. Sci. Eng. 8 (2), 135.
Hall, G.J., Frysinger, G.S., Aeppli, C., Carmichael, C.A., Gros, J., Lemkau, K.L., Nelson, R. K., Reddy, C.M., 2013. Oxygenated weathering products of Deepwater Horizon oil come from surprising precursors. Mar. Pollut. Bull. 75 (1), 140–149.
Heath, D.J., Lewis, C.A., Rowland, S.J., 1997. The use of high temperature gas chromatography to study the biodegradation of high molecular weight hydrocarbons. Org. Geochem. 26 (11), 769–785.
ITOPF (International Tanker Owner Pollution Federation), 2023. Oil Tanker Spill Statistics 2022. Available from: https://www.itopf.org/knowledge-resources/data-statistics/statistics/ (accessed 2023.09.30).
Ji, Y., Zeng, C., Ferronato, C., Chovelon, J., Yang, X., 2012. Nitrate-induced photodegradation of atenolol in aqueous solution: kinetics, toxicity and degradation pathways. Chemosphere 88 (5), 644–649.
Jing, L., Chen, B., Zhang, B., Zheng, J., Liu, B., 2014. Naphthalene degradation in seawater by UV irradiation: the effects of fluence rate, salinity, temperature and initial concentration. Mar. Pollut. Bull. 81 (1), 149–156.
Kang, H., Jung, Y., Kwon, J., 2019. Changes in ecotoxicity of naphthalene and alkylated naphthalenes during photodegradation in water. Chemosphere 222, 656–664.
Kennedy, J.J., Rayner, N.A., Atkinson, C.P., Killick, R.E., 2019. An ensemble data set of sea surface temperature change from 1850: the Met Office Hadley Centre HadSST.4.0.0.0 Data Set. J. Geophys. Res.-Atmos. 124 (14), 7719–7763.
Keramea, P., Spanoudaki, K., Zodiatis, G., Gikas, G., Sylaios, G., 2021. Oil spill modeling: a critical review on current trends, perspectives, and challenges. J. Mar. Sci. Eng. 9 (2), 181.
King, S.M., Leaf, P.A., Olson, A.C., Zito, P., Tarr, M.A., 2014. Photolytic and photocatalytic degradation of surface oil from the Deepwater Horizon spill. Chemosphere 95, 415–422.
Kong, L., Ferry, J.L., 2004. Photochemical oxidation of chrysene at the silica gel-water interface. J. Photochem. Photobiol. A Chem. 162 (2–3), 415–421.

Liu, Z., Sun, X., Fu, J., Liu, W., Cai, Z., 2023. Elevated nitrate promoted photodegradation of PAHs in aqueous phase: implications for the increased nutrient discharge. J. Hazard. Mater. 443, 130143.
Mao, K., Liu, C., Zhang, S., Gao, F., 2023. Reconstructing ocean subsurface temperature and salinity from sea surface information based on dual path convolutional neural networks. J. Mar. Sci. Eng. 11 (5), 1030.
Moriasi, D.N., Arnold, J.G., Van Liew, M.W., Bingner, R.L., Harmel, R.D., Veith, T.L., 2007. Model evaluation guidelines for systematic quantification of accuracy in watershed simulations. Trans. ASABE 50 (3), 885–900.
Niles, S.F., Chacon-Patino, M.L., Chen, H., McKenna, A.M., Blakney, G.T., Rodgers, R.P., Marshall, A.G., 2019. Molecular-level characterization of oil-soluble ketone/aldehyde photo-oxidation products by Fourier transform ion cyclotron resonance mass spectrometry reveals similarity between microcosm and field samples. Environ. Sci. Technol. 53 (12), 6887–6894.
Niles, S.F., Chacón-Patiño, M.L., Marshall, A.G., Rodgers, R.P., 2020. Molecular composition of photooxidation products derived from sulfur-containing compounds isolated from petroleum samples. Energy Fuel 34 (11), 14493–14504.
NRC, 2003. Oil in the Sea III: Inputs, Fate, and Effects, National Academies Press (US), Washington (DC).
O'Connor, M., Helal, S.R., Latch, D.E., Arnold, W.A., 2019. Quantifying photo-production of triplet excited states and singlet oxygen from effluent organic matter. Water Res. 156, 23–33.
Passow, U., Overton, E.B., 2021. The complexity of spills: the fate of the Deepwater Horizon oil. Annu. Rev. Mar. Sci. 13 (1), 109–136.
Payne, J.R., Phillips, C.R., 1985. Photochemistry of petroleum in water. Environ. Sci. Technol. 19 (7), 569–579.
Plata, D.L., Sharpless, C.M., Reddy, C.M., 2008. Photochemical degradation of polycyclic aromatic hydrocarbons in oil films. Environ. Sci. Technol. 42 (7), 2432–2438.
Reed, M., Johansen, Ø., Brandvik, P.J., Daling, P., Lewis, A., Fiocco, R., Mackay, D., Prentki, R., 1999. Oil spill modeling towards the close of the 20th century: overview of the state of the art. Spill Sci. Technol. Bull. 5 (1), 3–16.
Saeed, T., Ali, L.N., Al-Bloushi, A., Al-Hashash, H., Al-Bahloul, M., Al-Khabbaz, A., Al-Khayat, A., 2011. Effect of environmental factors on photodegradation of polycyclic aromatic hydrocarbons (PAHs) in the water-soluble fraction of Kuwait crude oil in seawater. Mar. Environ. Res. 72 (3), 143–150.
Sengupta, M., Xie, Y., Lopez, A., Habte, A., Maclaurin, G., Shelby, J., 2018. The national solar radiation data base (NSRDB). Renew. Sust. Energ. Rev. 89, 51–60.
Shankar, R., Shim, W.J., An, J.G., Yim, U.H., 2015. A practical review on photooxidation of crude oil: laboratory lamp setup and factors affecting it. Water Res. 68, 304–315.
Stout, S.A., Payne, J.R., Emsbo-Mattingly, S.D., Baker, G., 2016. Weathering of field-collected floating and stranded Macondo oils during and shortly after the Deepwater Horizon oil spill. Mar. Pollut. Bull. 105 (1), 7–22.
Vinogradova, N., Lee, T., Boutin, J., Drushka, K., Fournier, S., Sabia, R., Stammer, D., Bayler, E., Reul, N., Gordon, A., Melnichenko, O., Li, L., Hackert, E., Martin, M., Kolodziejczyk, N., Hasson, A., Brown, S., Misra, S., Lindstrom, E., 2019. Satellite salinity observing system: recent discoveries and the way forward. Front. Mar. Sci. 6, 243.
Wang, Z., Fingas, M., Lambert, P., Zeng, G., Yang, C., Hollebone, B., 2004. Characterization and identification of the Detroit River mystery oil spill (2002). J. Chromatogr. A 1038 (1–2), 201–214.
Wang, Q., Leonce, B., Seeley, M.E., Adegboyega, N.F., Lu, K., Hockaday, W.C., Liu, Z., 2020. Elucidating the formation pathway of photo-generated asphaltenes from light Louisiana sweet crude oil after exposure to natural sunlight in the Gulf of Mexico. Org. Geochem. 150, 104126.
Ward, C.P., Overton, E.B., 2020. How the 2010 Deepwater Horizon spill reshaped our understanding of crude oil photochemical weathering at sea: a past, present, and future perspective. Environ. Sci. Process Impacts 22 (5), 1125–1138.
Ward, C.P., Sharpless, C.M., Valentine, D.L., French-McCay, D.P., Aeppli, C., White, H.K., Rodgers, R.P., Gosselin, K.M., Nelson, R.K., Reddy, C.M., 2018. Partial photochemical oxidation was a dominant fate of Deepwater Horizon surface oil. Environ. Sci. Technol. 52 (4), 1797–1805.
White, H.K., Wang, C.H., Williams, P.L., Findley, D.M., Thurston, A.M., Simister, R.L., Aeppli, C., Nelson, R.K., Reddy, C.M., 2016. Long-term weathering and continued oxidation of oil residues from the Deepwater Horizon spill. Mar. Pollut. Bull. 113 (1), 380–386.
Xie, H., Xu, Q., Cheng, Y., Yin, X., Fan, K., 2023. Reconstructing three-dimensional salinity field of the South China Sea from satellite observations. Front. Mar. Sci. 10, 1168486.
Yan, X., An, J., Zhang, Y., Wei, S., He, W., Zhou, Q., 2023. Photochemical degradation in natural attenuation of characteristics of petroleum hydrocarbons (C10-C40) in crude oil polluted soil by simulated long term solar irradiation. J. Hazard. Mater. 460, 132259.
Yang, G.P., Lin, Z.F., Shun, X.C., Zhou, L.M., 2008. Study on the photochemical degradation of crude oil in aqueous solutions. Period. Ocean Univ. China 2008 163 (4), 623–626.
Yang, Z., Hollebone, B.P., Brown, C.E., Yang, C., Wang, Z., Zhang, G., Lambert, P., Landriault, M., Shah, K., 2016. The photolytic behavior of diluted bitumen in simulated seawater by exposed to the natural sunlight. Fuel 186, 128–139.
Yang, Z., Yang, C., Zhang, G., Shah, K., Chen, B., Hollebone, B.P., Jackman, P., Beaulac, V., 2022. Effects of asphaltenes on the photolytic and toxic behavior of bitumen and conventional oil products on saltwater. J. Hazard. Mater. 436, 129137.
Ye, L., Manning, A.J., Hsu, T., 2020. Oil-mineral flocculation and settling velocity in saline water. Water Res. 173, 115569.
Zhang, L., Xu, C., Chen, Z., Li, X., 2011. Effect of UV intensity and wavelength on photocatalytic degradation of polycyclic aromatic hydrocarbons. Adv. Mater. Res. 233-235 (1–3), 466–469.
Zito, P., Chen, H., Podgorski, D.C., McKenna, A.M., Tarr, M.A., 2014. Sunlight creates oxygenated species in water-soluble fractions of Deepwater horizon oil. J. Hazard. Mater. 280, 636–643.
Zito, P., Podgorski, D.C., Bartges, T., Guillemette, F., Roebuck, J.A., Spencer, R.G.M., Rodgers, R.P., Tarr, M.A., 2020. Sunlight-induced molecular progression of oil into oxidized oil soluble species, interfacial material, and dissolved organic matter. Energy Fuel 34 (4), 4721–4726.